RSC Advances

PAPER

View Article Online
View Journal | View Issue

Cite this: *RSC Adv.*, 2024, **14**, 794

Reactive processing-microstructure-mechanical performance correlations in biodegradable poly(lactic acid)/expanded graphite nanocomposites†

Mahdi Rahmanifard, Seyed Mohammad Hassan Khademi, Reza Asheghi-Oskooee, Tara Farizeh* and Farkhondeh Hemmati *

Reactive extrusion is a promising method to prepare biodegradable nanocomposites with enhanced modulus, strength and toughness. In this study, biodegradable extended nanocomposites based on poly(lactic acid) (PLA)/expanded graphite (EG) were prepared by melt-compounding using a co-rotating twin-screw extruder. Effects of EG loading, aspect ratio, delamination and dispersion state on the mechanical and thermo-mechanical properties of PLA/EG nanocomposites were investigated. Adding the largest EG (EGL) nanoplatelets, having the average particle size of 48.2 μm and aspect ratio of 19.5, to the PLA matrix enhanced the Young modulus, tensile strength, ultimate strain and tensile toughness of the extended PLA sample with benzoyl peroxide (BP) between 40–100%. The observed enhancements originated from restricted PLA molecular motions, assisted PLA crystallization and intensified BP activity in extending the PLA chains. In contrast, EG nanofiller (EGS), with the lowest aspect ratio and size, lowered the PLA relaxation time and accelerated the PLA crystallization. This type of EG showed the weakest reinforcing effect on PLA. For the EG type (EGM) with an intermediate size and aspect ratio, it was observed that the presence of the nanoparticles had a negligible effect on the PLA molecular dynamic and reduced the PLA crystallization rate. The highest impact strength was observed for the PLA/EGM nanocomposite at 1 phr loading.

Received 28th September 2023
Accepted 5th December 2023

DOI: 10.1039/d3ra06622c

rsc.li/rsc-advances

1. Introduction

Nowadays, there is a growing interest for utilization of natural polymers from renewable resources, both in terms of research and industrial aspects. In fact, the global concerns such as the depletion of fossil fuel resources, and air, soil and water pollution as well as the ever-increasing plastic waste have led to the motivation for utilizing more eco-friendly resources.[1,2] Poly(lactic acid) (PLA) is one of these natural polymers that is produced from renewable resources. This polymer has a high potential to replace synthetic polymers in various applications due to the properties such as biodegradability, biocompatibility and good processability and mechanical properties.[3] PLA is a transparent hard thermoplastic with favorable mechanical properties that makes it suitable for the production of films, containers, bottles, drug delivery systems and packaging. On the other hand, the inherent brittleness, relatively high-water vapor permeability, low glass transition temperature, and poor thermal stability restrict the potential applications of this polymer. To confront the mentioned limitations, additives such as crystallization nucleating agents, plasticizers and nano-sized reinforcement agents can be used.[4] Expanded graphite (EG) is one of the most widely used types of graphites, which has a worm-like structure with low density and high heat resistance. In order to benefit from the maximum improvement of properties with the presence of graphite in the polymer matrix phase, the graphite nanolayers should be well dispersed and expanded in the matrix. In 2010, Kim *et al.* investigated the thermo-mechanical and electrical properties of PLA-based nanocomposites containing EG. In this research, the Young's modulus of PLA increased up to 3 wt% of the nanofiller (62 MPa increased to 70 MPa). According to their observations, by adding EG, the thermal degradation temperature of PLA increased by 10 K.[5] At higher EG loadings, above a critical level, graphite nanoplatelets form multi-layer stacks owing to the interlayer van der Waals interactions. Thus, at higher EG loadings, the properties of EG-contained nanocomposites do not show any further improvements.[6] In 2012, Chieng *et al.* investigated the effect of graphene sheet nanoparticles on the mechanical properties of PLA/epoxidized palm oil (EPO) blends. Their findings demonstrated that the maximum tensile strength of

Caspian Faculty of Engineering, College of Engineering, University of Tehran, P.O. Box 43841-119, Guilan, Iran. E-mail: tara.farizeh@ut.ac.ir; f.hemmati@ut.ac.ir

† Electronic supplementary information (ESI) available. See DOI: https://doi.org/10.1039/d3ra06622c

PLA/EPO/EG nanocomposites was attained at 0.3 wt% of EG content. Incorporating EG into PLA/EPO blends at higher loadings led to a drop in the tensile strength.[7] Expansion of graphite layers causes a larger interfacial area between matrix and the reinforcement agent.[8,9]

In 2014, Valapa *et al.* studied the effects of temperature and sonication process on the expansion of EG platelets. By increasing the temperature of the thermal expansion process up to a certain level, the interfacial area of EG filler with matrix was heightened. Though higher temperatures brought about restacking of EG nanolayers.[10] Similarly, the EG loading influences the dispersion and delamination state of the nanoplatelets. In 2016, Kashi *et al.* conducted a research on the PLA-based nanocomposites using graphene nanosheets in different percentages from 0 to 15 wt%.[11] They showed that at low concentrations, graphene nanosheets have good dispersion in PLA. While at higher loadings of EG, the stress flow fields during melt-compounding process were not strong enough to delaminate the EG nanoparticles.

Mngomezulu *et al.* in 2017, investigated the effect of adding expanded graphite on the structural, mechanical and flame retardancy properties of PLA. The good interfacial interactions of nanofiller/matrix restricted the chain molecular motions and increase the PLA glass transition temperature. They observed that higher EG loadings caused lower heat of fusion and crystallinity degree, which originated from a non-uniform dispersion and distribution state of EG along with a weak interfacial adhesion between PLA and EG nanolayers.[12]

One of the drawbacks of using PLA-based products in an industrial scale is its thermal degradation during melt processing like extrusion. In order to compensate the negative effects of the molecular weight reduction of PLA, different additive like free-radical initiators and epoxy-based chain extenders have been applied in the PLA product formulation.[13,14] Additionally, the presence of nanofiller can improve the PLA final properties and melt strength owing to the potential nucleating role of nanofiller solid surfaces.[15] Similarly, it has been reported that the addition of EG nanoplatelets to PLA melt led to better foamability of matrix in continuous extrusion foaming process, owing to higher crystallization rate and improved melt strength of PLA in the presence of the nanofiller.[16]

In this research, PLA nanocomposites have been prepared by using expanded graphite as an inexpensive nanofiller and a peroxide initiator to modify the structure and molecular weight of PLA chains through the continuous extrusion process using a twin-screw extruder. Although there are some published works about the properties of the PLA/EG nanocomposites in the literature, the correlations between the phenomena involved the melt processing and the morphology and final performance of these systems have been rarely considered. So, the main objective of this work is studying the correlations among the mechanical and thermo-mechanical properties, phenomena involved in the melt processing and morphology of the PLA/EG nanocomposites. In order to achieve this goal, the PLA molecular weight and structure, molecular dynamics and crystallization behavior in the presence of EG nanofillers with different aspect ratio and sizes have been investigated. It will be shown that EG aspect ratio and particle size have profound impacts on the PLA molecular dynamics, crystallization rate and the chain extension activity of the free-radical initiator. It will be demonstrated that these phenomena improve all mechanical properties of PLA including elastic modulus, tensile strength and toughness.

2. Experimental part

2.1. Materials

In this research, commercial poly(lactic acid), grade 5Ö BIOKAS, by Chemic Kas LLC (Austria) was used. Moreover, graphite powder with three different initial particle sizes were used: (a) graphite powder with initial particle size smaller than 50 μm manufactured by Merck company (Germany) (GM), (b) graphite powder with average initial particle size of 90 μm manufactured by Sin Chem company (South Korea) (GK) and (c) graphite flake with initial particle size 500 μm manufactured by Shandong Qingdao Co. (China) (GF). Sulfuric acid and nitric acid were supplied by Kimia Tehran Acid Company (Iran) used to modify graphite and obtain expanded graphite. Benzoyl peroxide (BP) by Merck (Germany) was applied in the extrusion process to compensate for the decrease in the PLA molecular weight.

2.2. Sample preparation

2.2.1. Thermal expansion of graphite flake and powder. Three types of graphite, as mentioned above, were used in this research. In order to obtain expanded graphite, graphite powder/flake was modified using intermediate acidic compounds. To this aim, 10 g of graphite was dispersed in 200 ml sulfuric acid in a beaker, followed by slowly adding 100 ml of nitric acid to the solution. The beaker was placed in an ice-water bath to control the temperature of the reaction medium. The nature of this reaction, especially in the early hours, is exothermic. After 24 hours, the graphite was separated from the acid mixture by a filter paper and washed with distilled water for several times. A Buchner funnel was used to completely separate graphite from solvents and distilled water in this step. Furthermore, the intercalated graphite was placed in a vacuum oven for 24 hours to dry completely. The dried graphite was gently separated from the filter paper and crushed into small particles. The crushed particles are then placed in a furnace with a temperature of 1000 °C for 30 s to cause the explosive evaporation of acids from the graphite inter-layer galleries. After thermal shock, more bulky expanded graphite has been obtained. In fact, the volume of the graphite and the distance between the graphite platelets increase significantly. Through this preparation process, the structure of graphite powder/flake changed from the graphite sheets to honeycomb structure.

It is noteworthy that in this paper, letter E is used for the expanded material, and letter G is used to show graphite. Moreover, letter L shows for graphite with a large aspect ratio, letter M is for the graphite with a medium aspect ratio, and S is for the graphite with a small aspect ratio.

2.2.2. Preparation of PLA/EG nanocomposites. Masterbatches of PLA and EG were prepared, in order to disperse the graphite nanolayers well in the PLA matrix. To this aim, PLA and graphite were first dried in a vacuum oven at 60 °C for 12 hours. Afterwards, the melt-compounding of 20 phr of expended graphite in the PLA matrix phase were done by using a co-rotating twin-screw micro-extruder (Rondol company, UK) at a screw speed of 150 rpm. During the melt-compounding of 20 phr of EGs with PLA, high melt viscosity, screw torque and die pressure were observed, especially for the melt-compounding of 20 phr of EGL (with largest particle size) with the PLA matrix. Therefore, the barrel temperature profile used for the PLA/EGL masterbatch was higher than the temperature profile applied for the PLA/EGM and PLA/EGS masterbatches. The temperature profile for preparing the PLA/EGM and PLA/EGS masterbatches was 165, 160, 170, 175, 175 °C, from hopper to die. While, for PLA/EGL masterbatch, the temperature profile was 165, 160, 170, 185, 185 °C. In order to prepare the PLA/EG nanocomposites, a certain amount of prepared masterbatches, pure PLA granules and benzoyl peroxide were dried in a vacuum oven at 60 °C for 12 hours. The samples were prepared with 1, 3, 5, 7, 9, 11, 15 and 20 phr of EG and 0.5 phr of benzoyl peroxide by using the twin-screw micro-extruder, at the temperature profile of 140, 160, 145, 155, 155 °C from hopper to die, at a screw speed of 150 rpm. The extruder was equipped with a rod-shaped die. The extruded nanocomposite rods were cooled in a water bath, then granulized. Afterwards, the nanocomposite granules were molded by a compression-molding machine. The specimens for tensile, Vicat and impact tests were obtained by applying this molding machine at a temperature of 180 °C and a pressure of 180 MPa. It should be noted that the cooling process for the molded nanocomposites sheets were done quickly by using a water bath. Because of using two different barrel temperature profiles for melt-compounding of the PLA/EG masterbatches, two PLA/BP control samples were obtained in the same processing conditions (masterbatch extrusion process + nanocomposite extrusion process). These two control samples were characterized in each experiment along with the obtained PLA/EG nanocomposites. The experimental data obtained for the PLA/EG nanocomposites were normalized by dividing the data related to the nanocomposites by the data belong to the corresponding PLA/BP control sample. The normalized data are reported in the following parts. In the rest parts, the nanocomposites will be coded as PLAEG*x*, where *x* stands for the EG loading in phr (parts per hundred parts of resin, PLA).

2.3. Characterization

The density of the prepared samples was measured by using the solvent-displacement method following ASTM D792. *N*-Hexane with the density of 0.66 g cm^{-3} at 25 °C was used as solvent in the measurements. The granules after the melt-compounding process in the extruder were applied for each measurement. In order to determine the temperature of the Vicat softening point, the SHV-303 device (Santam LLC, Iran) was used, and the test conditions were performed according to the ASTM D1525 standard. The rectangular specimens with dimensions of 22.5 × 22.5 × 4.25 mm^3 were prepared by the compression molding machine (the processing conditions were mentioned in the previous subsection). At least three specimens were molded and the average of Vicat softening points of at least three samples was reported. Tensile test was performed by universal tensile device (Sanaf LLC, Iran) according to ASTM D638 standard with the stretching speed of 1 mm min^{-1}. The dumbbell-shaped specimens (type VI of ASTM D638) were used for tensile stress–strain test. The specimens were punched from the compression-molded sheets with average thickness of 1 mm. Five sheets were molded for each sample. The reported tensile properties are the average results of at least 5 replicates. To determine the impact strength, the SIT-20E device (Santam LLC, Iran) was used. The Izod pendulum test was performed in accordance with ASTM D256. All the tests were done at the temperature of 20 °C on notched bars. The depth of each notch was 2.5 mm, and was prepared by the BHO_CB device (Santam LLC, Iran). The rectangular bars with dimensions of 63.5 × 15 × 10 mm^3 were obtained by the compression molding machine. Ten specimens were molded and the average of Izod impact strength of at least four samples was reported.

In order to investigate the EG morphology as well as the dispersion and distribution state of EG nanoparticles in the PLA matrix, electron microscope images were applied (SEM TESCAN VEGA, Czech Republic). The nanocomposites were cryogenically fractured in liquid nitrogen bath and gold-sputtered before being exposed to electron beam. The linear viscoelastic properties of PLA matrix and PLA/EG nanocomposites were evaluated by isothermal frequency sweep tests at fixed temperature of 170 °C and a strain of 1% using Anton Paar parallel-plate

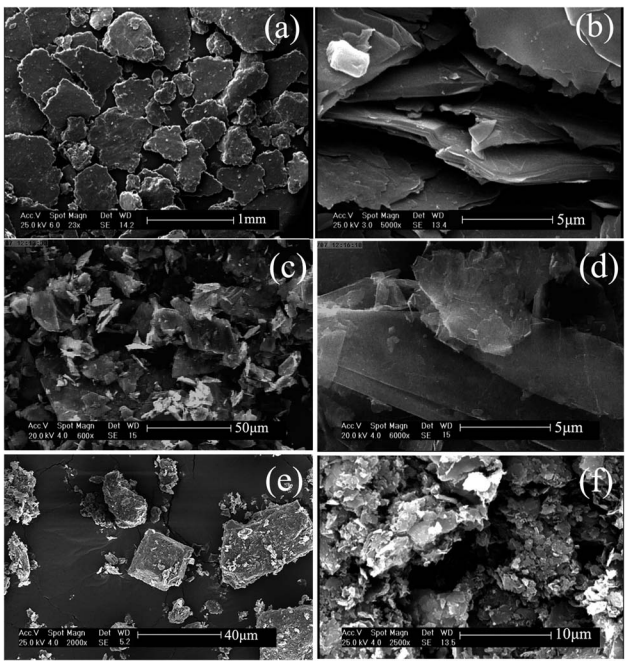

Fig. 1 SEM images of different types of graphite before and after thermal shock. The images on the left side are the graphite fillers before thermal shock and the images on the right show the expanded graphite particles. (a) GF, (b) EGL, (c) GM, (d) EGM, (e) GK, (f) EGS.

rheometer (MCR30, Austria) with a constant gap of 1 mm and plate diameter of 25 mm on the molded sheets. All the experiments were performed under highly pure nitrogen atmosphere. The molecular weight of PLA chains in the presence and absence of BP and EG was measured using gel permeation chromatography (GPC, Agilent, USA) with tetrahydrofuran solvent as carrier. The crystallization kinetics of PLA in the presence of EGs was isothermally studied by using Mettler Toledo differential scanning calorimetry (DSC) (DSC1 model, Switzerland). The specimens, with a weight of 5–10 mg, were heated to 180 °C with a heating rate of 10 °C min^{-1}. Then, the samples were held for 5 min at 180 °C for erasing the thermal history. Next, the samples were quenched to 118 °C and isothermally kept at 118 °C to complete the isothermal crystallization peak of PLA. The tests were conducted under highly pure nitrogen atmosphere with a volume flowrate of 80 ml min^{-1}.

3. Results

3.1. Structural properties

Scanning electron microscopy (SEM) images of different used graphites here are shown in Fig. 1. The images can be applied to clarify the success of thermal shock in the expansion of graphite nanolayers. As can be seen in Fig. 1, GF graphite, which had the largest primary particle size before the thermal shock (500 micrometers), has also the largest aspect ratio among others after the expansion process. This EG is named as "EGL" in the following parts. Scanning electron microscopy (SEM) images of different used graphites here are shown in Fig. 1.

The images can be applied to clarify the success of thermal shock in the expansion of graphite nanolayers. As can be seen in Fig. 1, GF graphite, which had the largest primary particle size before the thermal shock (500 micrometers), has also the largest aspect ratio among others after the expansion process. This EG

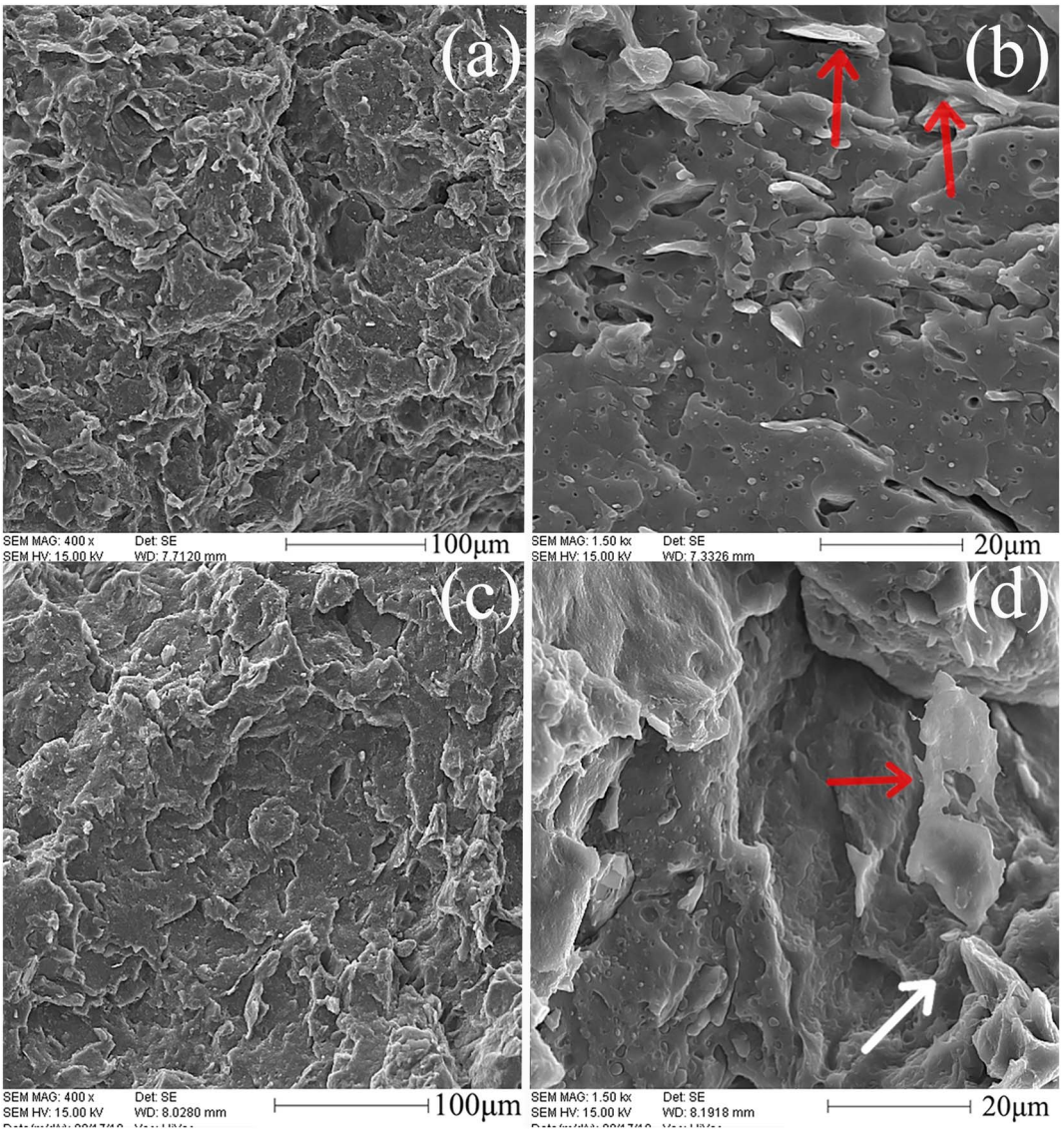

Fig. 2 SEM images of PLA/EGM nanocomposites: (a) and (b) PLAEGM1, (c) and (d) PLAEGM9. The images in the right column are the higher magnification of left images.

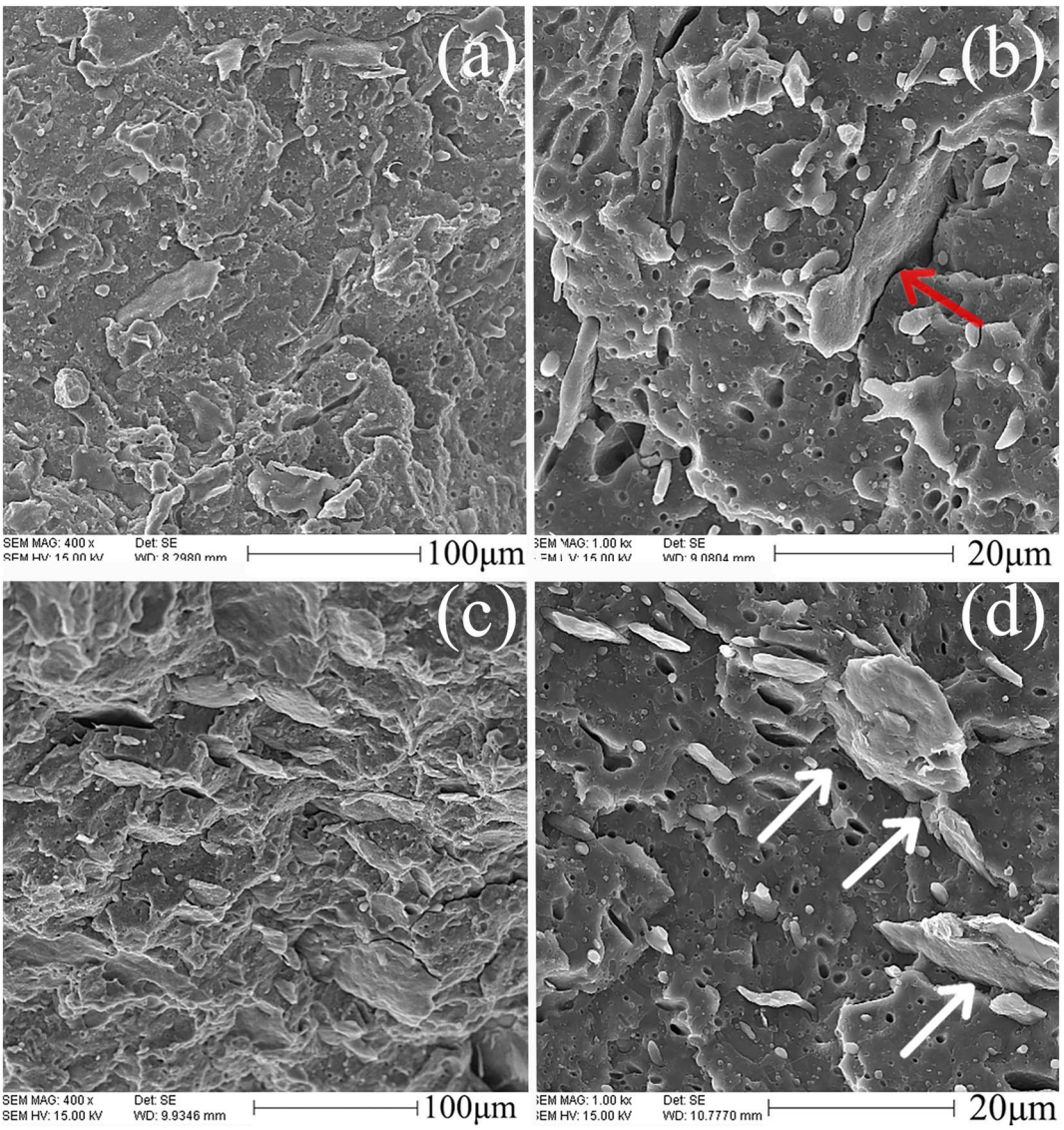

Fig. 3 SEM images of PLA/EGL nanocomposites: (a) and (b) PLAEGL1, (c) and (d) PLAEGL9. The images in the right column are the higher magnification of left images.

is named as "EGL" in the following parts. The average size for EGL platelets was 48.2 ± 14.1 μm and the aspect ratio of EGL particles was 19.5 ± 7.6. The average size and aspect ratio for GM graphite after thermal shock (shown by EGM), were respectively equal to 46.2 ± 4.8 μm and 8.9 ± 0.1. However, thermal shock did not have significant effect on GK graphite and almost no expansion is observed in the images. The particle size and aspect ratio for this graphite type (shown by EGS) reached to 1.5 ± 0.3 μm and 12.3 ± 2.5 respectively, which is the smallest type of used graphite after thermal shock. Distribution and dispersion of EG nanoplatelets in the PLA matrix are among the main parameters that affect the physical, mechanical and structural properties of the nanocomposite. Fig. 2 shows the SEM images of the nanocomposites containing EGM filler. Fig. 3 and 4 show the cryo-fractured surfaces of PLA/EGL and PLA/EGS nanocomposites, respectively. It is clear in Fig. 2–4 that the graphite particles in the nanocomposites have the same order in size as the EGs have before the melt-compounding process. It seems that the applied melt-compounding process reduces the size of EG nanoparticles. The thin EG stacks and single layers are marked by red arrows in the SEM images. One may also observe that the surface of graphite layers is covered with a layer of PLA (see Fig. 3(b) and (d)), which indicates good wetting of EG particles with PLA matrix. This phenomenon can be also discerned in Fig. 2 and 4. Moreover, it can be also deduced that in the SEM images of samples having 9 phr of expanded graphite, multi-layer stacks remained in the matrix after the melt-compounding process. These multi-layer stacks, which are placed very close to each other, are marked by white arrows in the images. At higher nanofiller loadings, the stresses that are present in the extrusion process are not strong enough to completely delaminate the EG stacks. Therefore, the dispersion and distribution of EG nanoplatelets become weaker at higher EG loadings. Additionally, the SEM images demonstrate

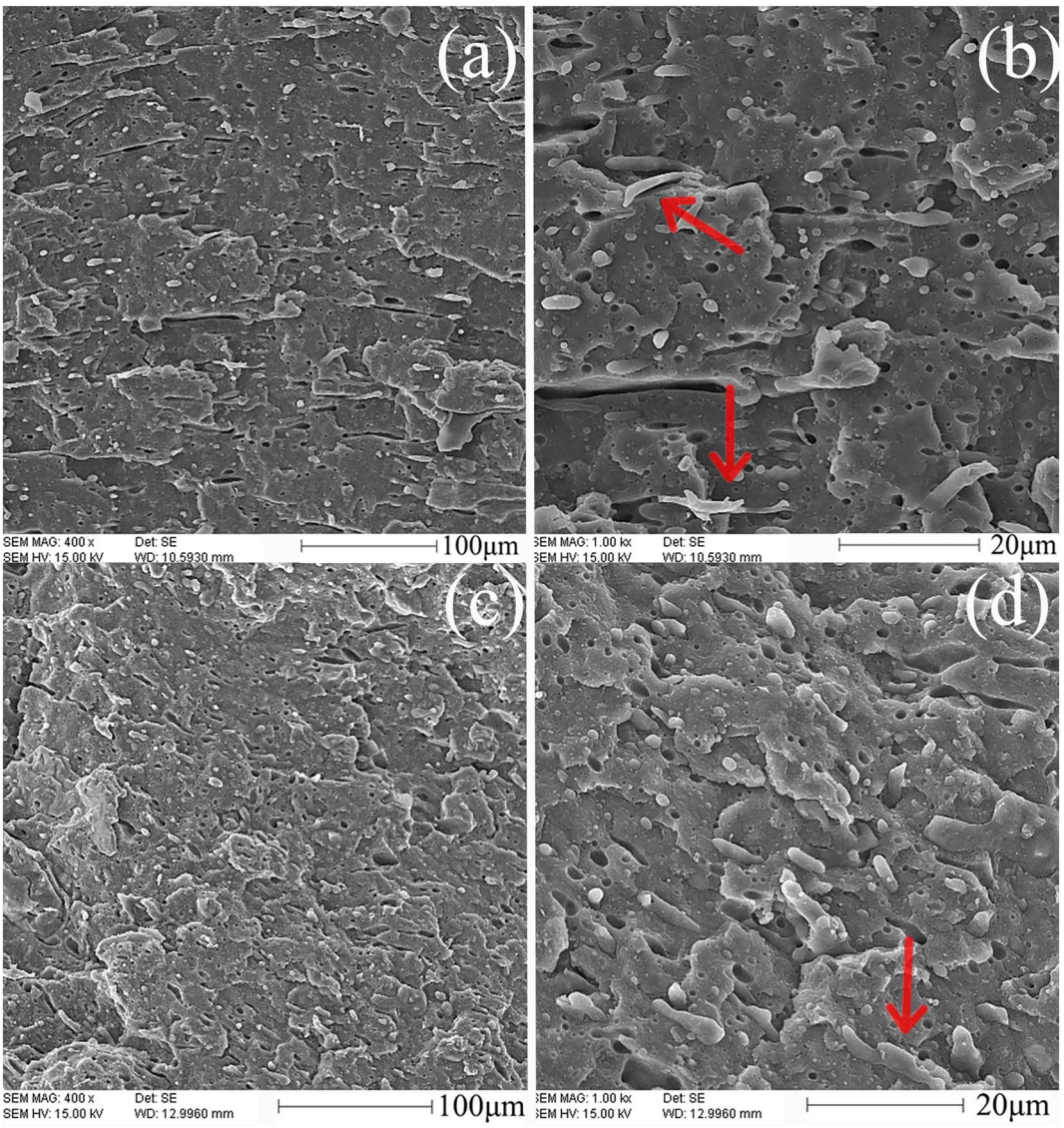

Fig. 4 SEM images of PLA/EGS nanocomposites: (a) and (b) PLAEGS1, (c) and (d) PLAEGS9. The images in the right column are the higher magnification of left images.

that the cryo-fractured surfaces of the PLA/EGM and PLA/EGL nanocomposites are rougher than that of the PLA/EGS samples. The rougher surface confirm that the EGL and EGM nanoparticles comparatively influence the PLA matrix to higher extents.[17]

3.2. Mechanical properties

3.2.1. Tensile stress–strain test. Tensile stress–strain tests were performed on the nanocomposites and the mechanical characteristics of the nanocomposites were normalized to the corresponding characteristics of the processed PLA/BP specimens as control samples. The normalized mechanical characteristics including Young modulus, tensile strength, elongation at break and dissipated energy (obtained by integrating the area under stress–strain curve) are represented in Fig. 5–8. It is clear from Fig. 5 that the highest values of the tensile modulus correspond to the samples with EGL nanoparticles. Among other EGs, the best reinforcement agent for the PLA matrix is EGL with highest aspect ratio and particle size. Better expansion of EG nanofiller plus larger particle size and aspect ratio result in largest filler/matrix interfacial area for EGL. The larger interfacial area for stress transfer in PLA/EGL nanocomposites causes considerable higher Young modulus for these nanocomposites. A closer look at Fig. 5 reveals that the Young modulus of PLA/EGM nanocomposites places at the second step. The lowest elastic modulus belongs to the PLA/EGS nanocomposites containing smallest EG nanoparticles. In addition, one may deduce from Fig. 5 that by increasing the filler loading up to 20 phr, the improvement of elastic modulus becomes less noticeable. A drop in elastic modulus by incorporating higher levels of EG is observed for all used EG nanofillers here. The plausible reason is the accumulation of graphite stacks and layers as well as the possibility of less opening of the EG inter-layer galleries at higher percentages of

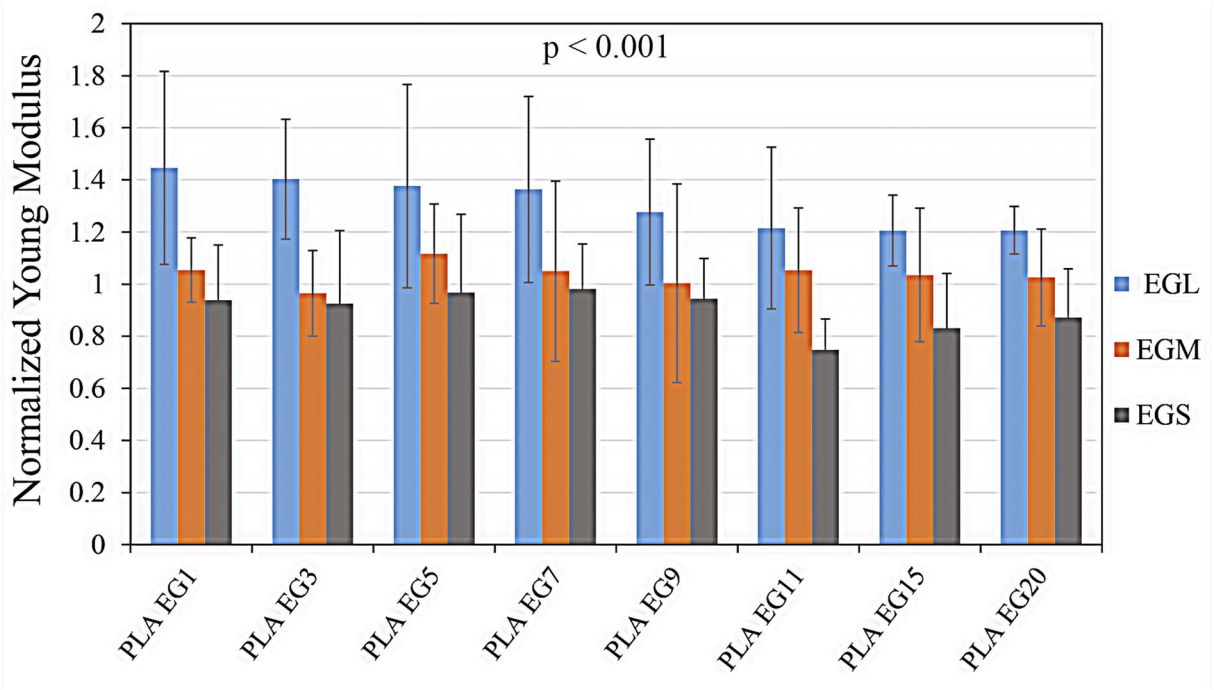

Fig. 5 Normalized Young modulus for: PLAEG1, PLAEG3, PLAEG5, PLAEG7, PLAEG9, PLAEG11, PLAEG15, and PLAEG20. The *p*-value of data is shown in the graph.

filler in a certain stress flow field. The similar trends can be also observed for the tensile strength property, which is clearly evident in Fig. 6. The samples, which contain the EGs with higher aspect ratio (EGM and EGL), show larger tensile strength. This is due to the greater contact surface area of the filler platelets with the PLA matrix. As can be observed, the

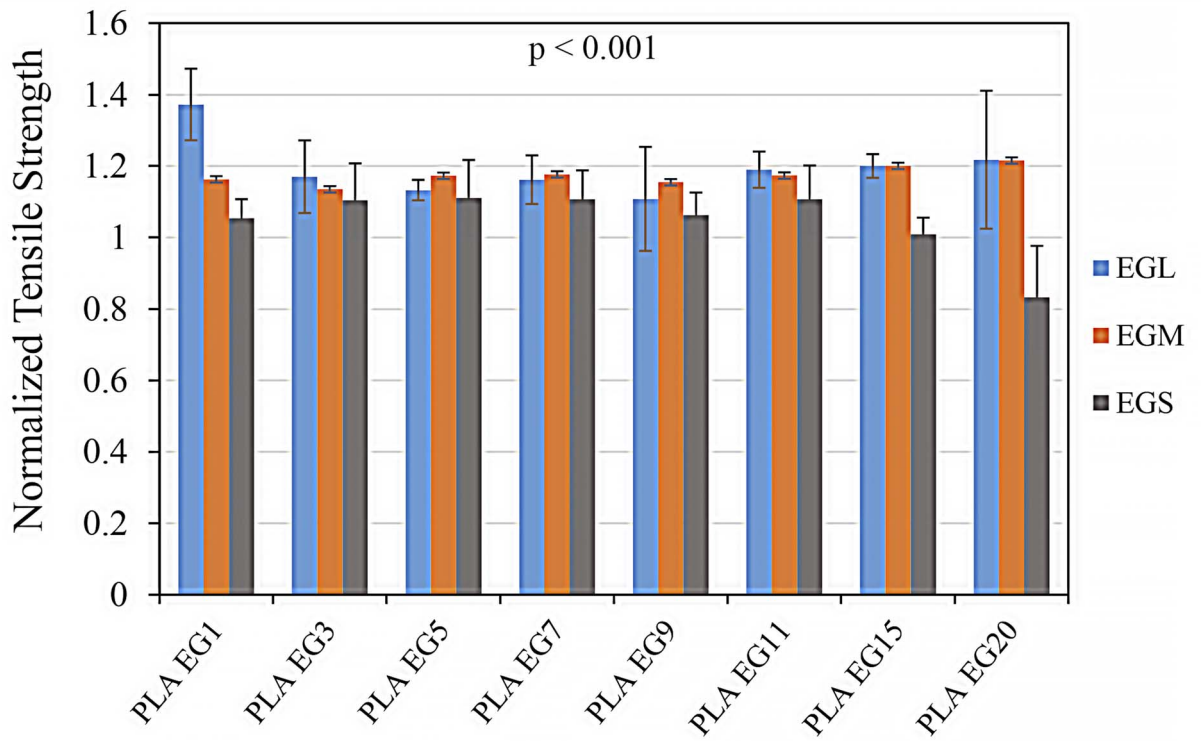

Fig. 6 Normalized tensile strength for: PLAEG1, PLAEG3, PLAEG5, PLAEG7, PLAEG9, PLAEG11, PLAEG15, and PLAEG20. The *p*-value of data is shown in the graph.

normalized tensile strength of PLA/EGS nanocomposites are lower than the ones for PLA/EGL and PLA/EGM sheets. The nanolayers in EGS stacks did not open well during the sample preparation process. Hence, the lowest reinforcing effect of EG nanofillers on PLA was observed for the PLA/EGS nanocomposites. The largest tensile strength is attained for PLAEGL1 nanocomposite, which contain the largest EG particles at the lowest loading (1 phr). In contract to PLA/EGS samples, the tensile strength of other nanocomposites, PLA/EGM and PLA/EGL, reduces by EG loading first, then increases. By increasing the EG content, the multilayer stacks and particle accumulation influence the tensile strength of samples negatively. However, further increment in the EG loading results in a slight improvement in the ultimate stress. The larger quantity of EG nanoparticles, loadings around 20 phr, can probably compensate the negative effects of EG accumulation and poor delamination on the strength. However, EG nanofiller, particularly at good dispersion state, can influence the PLA crystallinity, molecular dynamics as well as the extent of BP-induced reaction.

Fig. 7 and 8 respectively demonstrate normalized elongation at break and dissipated energy for various prepared samples. The dissipated energy, as a criterion for the toughness of sample during tensile stress–strain test, is determined by the integration of the area under stress–strain curve. It is clear from these figures that just the samples containing EGL filler have larger strain at break and tensile toughness than PLA/BP sample, the control sample. While the presence of EGL nanoplatelets in the extended PLA matrix with BP results in larger elastic modulus and tensile strength, the EGL addition leads to higher tensile toughness and ultimate strain as well. For most reinforcement agents, the later cannot be obtained.[18–20] It has been reported that by attaining optimal dispersion state of nanoparticles in a polymeric matrix through applying an adequate processing and fabrication method, improved reinforcement effect of nanofiller will be observed.[20] Better dispersion and delamination of EGL comparing to the other EGs are two reasons that obtaining higher mechanical properties. However, the effects of EGL presence on the chemical reaction of the used free-radical initiator with PLA chains, PLA crystallization behavior and PLA molecular dynamics can improve the mechanical performance of PLA as well. These effects will be thoroughly discussed in the "Discussion" part. Meanwhile, for the EGS nanofiller with the lowest matrix-filler interfacial area, which the EG stacks have not been opened very well in the expanding process, the lowest tensile characteristics are observed among the prepared nanocomposites. Especially higher loadings of EGS bring about even weaker mechanical performance in the tensile stress–strain test. The other type of expanded graphite, EGM, with an intermediate particle size and filler/matrix interfacial area, does not cause increments in the elongation at break and dissipated energy, contrary to the Young modulus and tensile strength. The EGM nanofiller changes the tensile toughness and strain at break in an opposite way from EGL. In the following parts, it will be shown that these differences originate from reverse influences of EGM and EGL on the PLA crystallization rate and molecular dynamic.

3.2.2. Impact pendulum test. Fig. 9 depicts the normalized impact strength of samples containing 1, 5 and 9 wt% of expanded graphite. As can be seen, the impact strength of the nanocomposites is lower than that of the control sample, PLA/BP, indicating the negative effect of EG on the impact

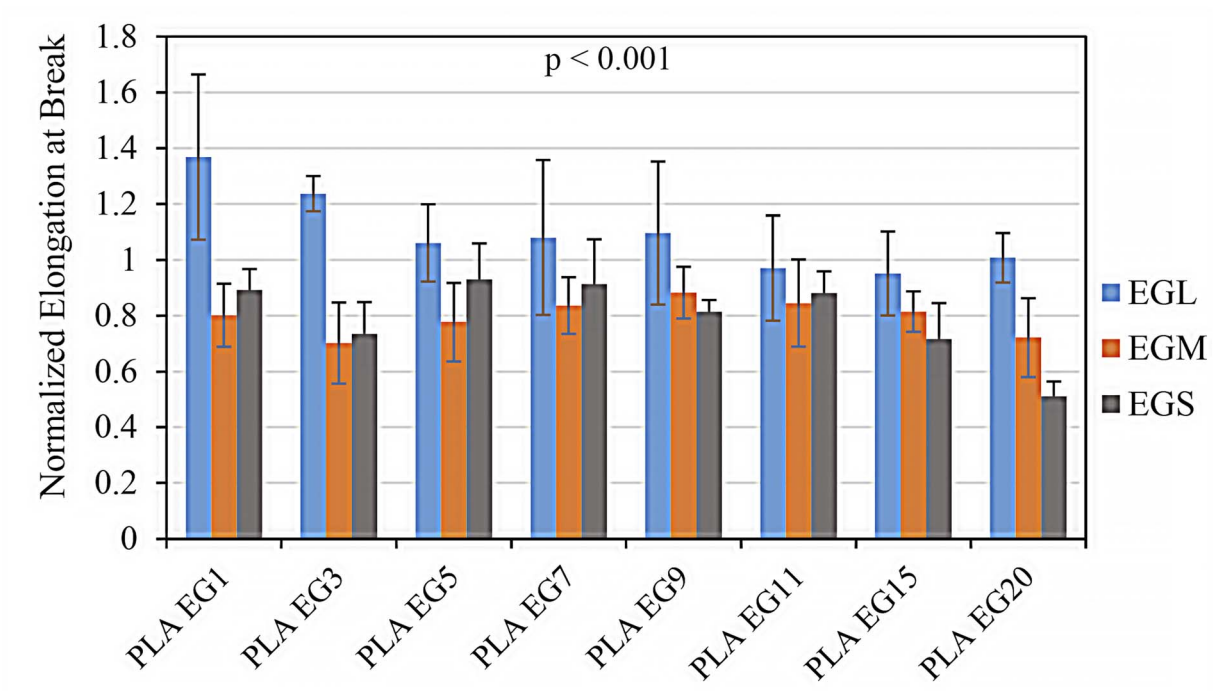

Fig. 7 Normalized elongation at break for: PLAEG1, PLAEG3, PLAEG5, PLAEG7, PLAEG9, PLAEG11, PLAEG15, and PLAEG20. The *p*-value of data is shown in the graph.

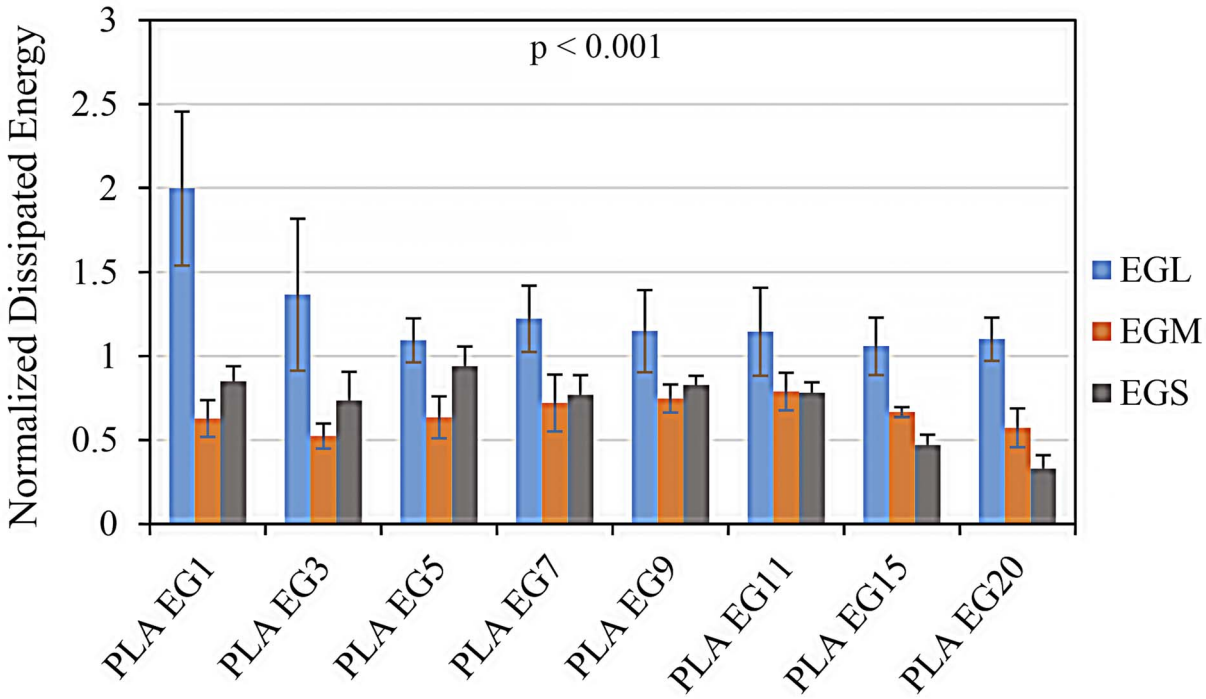

Fig. 8 Normalized dissipated energy for: PLAEG1, PLAEG3, PLAEG5, PLAEG7, PLAEG9, PLAEG11, PLAEG15, and PLAEG20. The *p*-value of data is shown in the graph.

strength of PLA. The only exception here is PLAEGM1, which shows higher impact toughness than PLA/BP sample. The effect of added graphite nanoplatelets on the impact strength of the PLA matrix can be addressed in two ways. First, added expanded graphite may lead to a decrease in the PLA crystallinity degree or crystal size, which result in higher impact toughness. Second, the EG nanolayers affect the molecular dynamics of PLA chain by absorbing the macromolecules on the solid surfaces. These

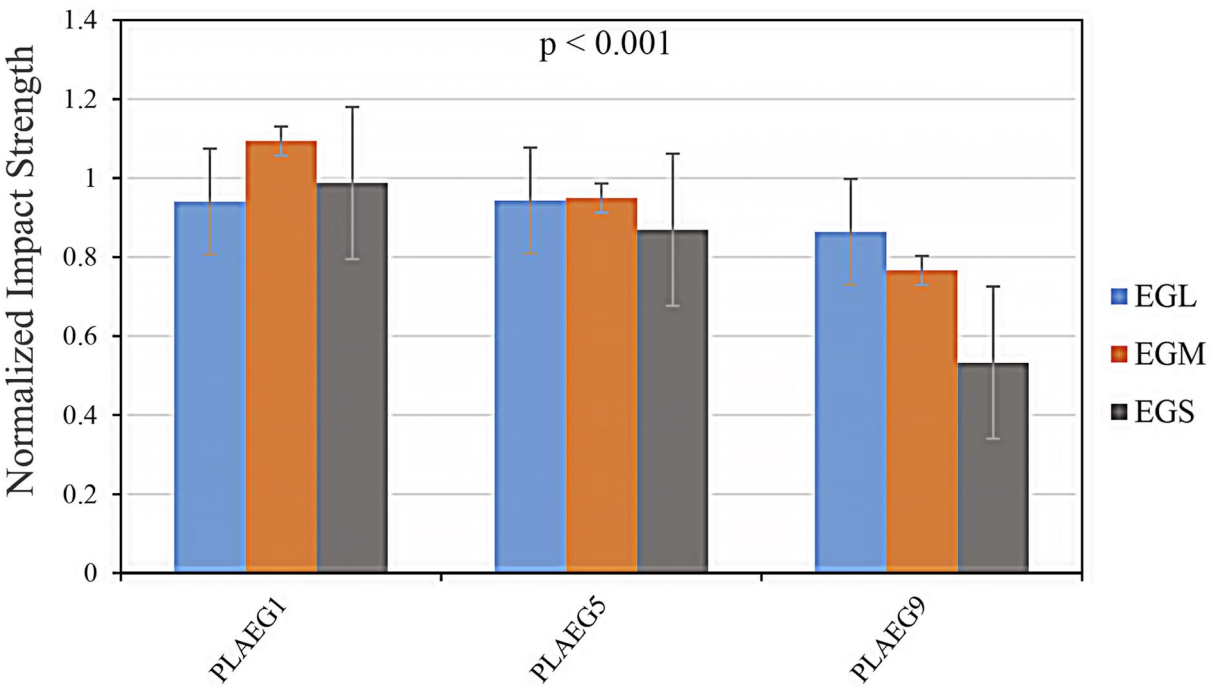

Fig. 9 Normalized impact strength for: PLAEG1, PLAEG5, and PLAEG9. The *p*-value of data is shown in the graph.

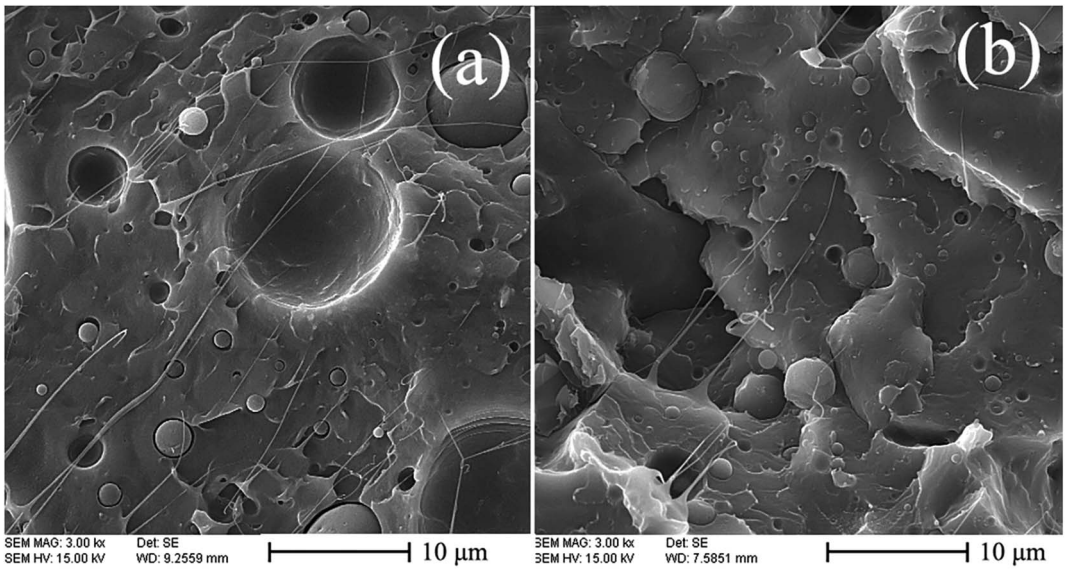

Fig. 10 SEM micrographs on impact fractured surface of the PLA/EGM nanocomposites: (a) PLAEG1, and (b) PLAEG9.

two effects together determine the impact strength of the nanocomposites, which will be investigated in the discussion part. Although the EG nanoplatelets influence the PLA impact toughness in opposite way, all prepared nanocomposites show lower strength by increasing the EG loading. The EG agglomerations and larger multilayer stacks themselves can act as stress concentrators and reduce the PLA impact strength by providing larger voids at filler/matrix interfaces.[19,21,22] Consequently, a descending trend in impact toughness is observed for all prepared nanocomposites. It is worthy to note that for EGS samples, the larger drop in impact toughness is observed, which originates from the poor delamination and dispersion state of this nanofiller. The SEM images of the impact fractured surfaces of PLAEGM1 and PLAEGM9 are shown in Fig. 10. It can be seen that the extent of the plastic deformation and fibrillation are decreased by increasing the EG loading. At higher nanofiller levels, energy absorption mechanisms are weakened owing to the nanofiller accumulation.[19–21]

3.3. Thermo-mechanical property

Vicat softening points of PLAEG1, PLAEG11 and PLAEG20 nanocomposites were measured and normalized by the ones for the PLA/BP samples. The obtained data are shown in Fig. 11. The Vicat softening temperatures of PLA/BP samples were about to 60 °C. It is clear from Fig. 11 that this temperature did not change significantly for the nanocomposite samples. Moreover, the corresponding temperature of the samples filled with EGL is comparable with the PLA/BP one. While, the other nanocomposites show lower Vicat softening points than the control samples. Additionally, further reduction in the softening temperature can be observed for the higher loadings of EGs. This is owing to the lack of proper wetting of the filler particles with the PLA matrix at high levels of EG nanofillers, which results from the accumulation of filler particles next to each other. As can be found in Fig. 11, the softening temperature of the nanocomposites decreases with a reduction in the EG aspect ratio.

3.4. Physical property

The density of prepared sample was measured and the normalized values of the PLA/EG nanocomposites were calculated by dividing the density of the nanocomposites by the density of the corresponding PLA/BP control sample. The results are shown in Fig. 12. As can be seen, the densities of the prepared PLA/EG nanocomposites are close to the density of the PLA/BP samples. By increasing the EG loading, the larger densities for the nanocomposites are obtained. It is noteworthy that the *p*-values of data in Fig. 5–9 as well as Fig. 11 and 12 are all less than 0.001, indicating the changes of the properties against the EG type and loading are statistically significant. In

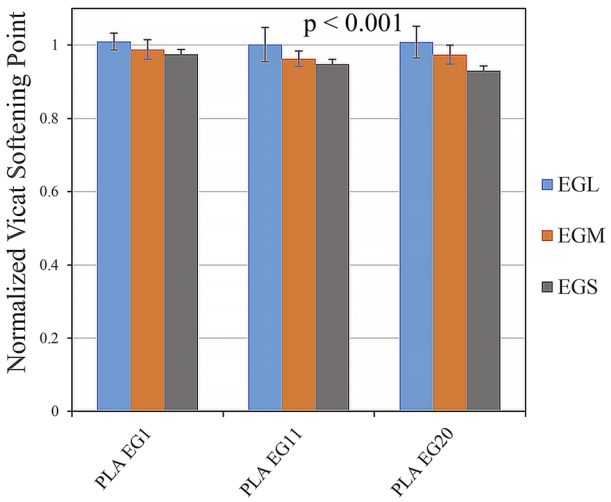

Fig. 11 Normalized Vicat softening point of: PLAEG1, PLAEG11, and PLAEG20. The *p*-value of data is shown in the graph.

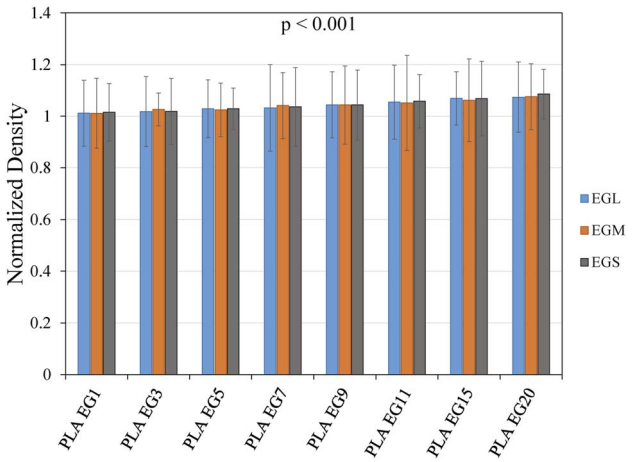

Fig. 12 Normalized density for: PLAEG1, PLAEG3, PLAEG5, PLAEG7, PLAEG9, PLAEG11, PLAEG15, and PLAEG20. The *p*-value of data is shown in the graph.

addition, the *p*-values for each reported data in these graphs are calculated and gathered in Tables S1 to S6 in the ESI† part. Roughly, all these *p*-values are less than 0.05.

4. Discussion

The observed changes in the mechanical properties of different PLA/EG nanocomposites are resulted from the changes in the PLA crystallinity, benzoyl peroxide activity in the presence of EG nanoplatelets and PLA molecular movements. As shown earlier, the used EGs here have different sizes and aspect ratio. The agglomeration and stack size, delamination state and filler/matrix interfacial area have been different in PLA/EGS, PLA/EGM and PLA/EGL nanocomposites. Hence, different EGs affects the PLA crystallization rate, BP chain extending activity and PLA chain dynamics to different extents. These phenomena cause the observed changes in the mechanical properties of PLA. The molecular motion of PLA macromolecules was studied by measuring the linear viscoelastic properties of samples through the isothermal rheological frequency sweep tests. The obtained data are shown in Fig. 13. As can be found, the viscoelastic properties of PLA/BP control sample, including storage modulus (G'), loss modulus (G'') and complex viscosity (η^*), are altered differently by incorporating different EGs, especially in the low-frequency region.

While the addition EGM nanolayers to PLA/BP sample does not cause any noticeable changes in the viscoelastic properties, the presence of EGL nanoplatelets, with the largest aspect ratio and filler/matrix interfacial area, improve the rheological properties considerably. Among different EGs, just EGS nanofiller, having the lowest aspect ratio and poor delamination state, shows an adverse influence on the PLA/BP viscoelastic properties. The relaxation time of PLA macromolecules was evaluated by determining the cross-over frequency (ω_r) of samples, *i.e.* the frequency at which the dynamic moduli (G' and G'') are equal to each other. The inverse of cross-over frequency is the longest relaxation time (τ_r) of the matrix molecules, $\tau_r = (\omega_r)^{-1}$.[23,24] This relaxation time were determined accordingly and gathered in Table 1. The data in Table 1 clarify that different EGs have different impacts on the molecular movements of PLA macromolecules. The best interactions between PLA and EG nanofiller belongs to EGL, with largest nanoplatelet size and interfacial area. As can be seen, PLAEGL3 nanocomposite has the largest relaxation time. In contrast, the EGS nanofiller, having poor delamination and dispersion state,

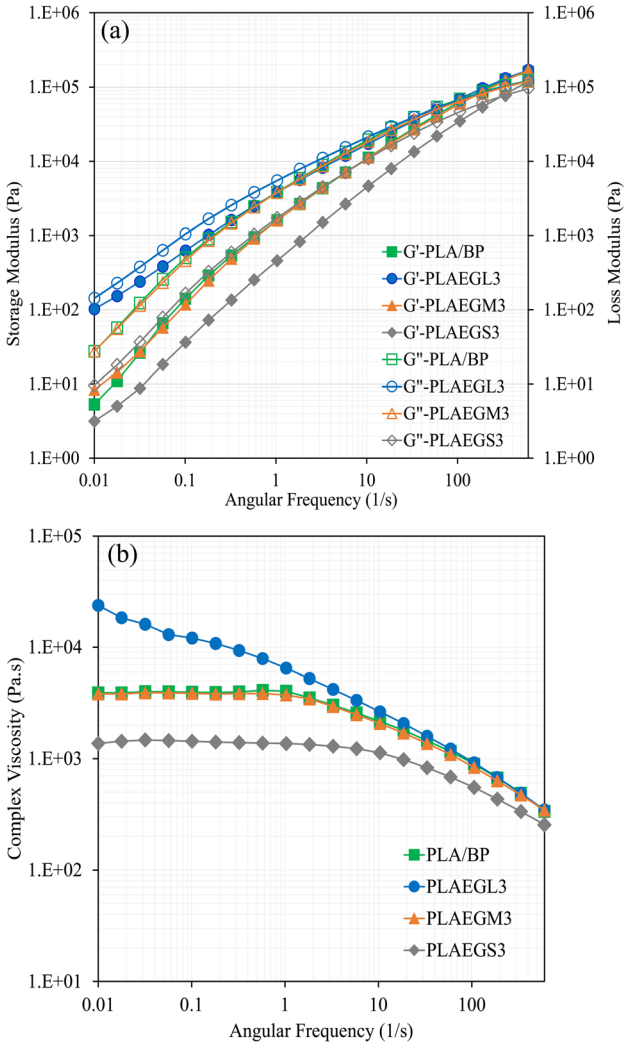

Fig. 13 (a) Dynamic moduli including storage and loss moduli against frequency, (b) complex viscosity against frequency determined by isothermal frequency sweep test at 170 °C and a linear strain of 1%.

Table 1 Cross-over frequency and longest relaxation time of PLA chains in different samples

Sample	Cross-over frequency (s^{-1})	Longest relaxation time (ms)
PLA/BP	152	6.6
PLAEGL3	83	12
PLAEGM3	148	6.7
PLAEGS3	290	3.4

show even shorter relaxation time than the control sample, PLA/BP. It seems that the EGS nanoparticles disturb the packing of the PLA chains and bring about faster molecular movements. Nonetheless, EGM does not alter the relaxation time of PLA macromolecules noticeably. Therefore, the best reinforcing effect of EG nanofillers on the PLA matrix is related to EGL and the worst reinforcing influence belongs to EGS. The incorporation of EG nanofillers into PLA not only affects the amorphous parts of the matrix, but can also impact the crystalline regions of PLA as well. These influences are both critically important in the mechanical performance of the nanocomposites.[25,26] It has been reported that the addition of PLA-grafted cellulose nanocrystals to PLA remarkedly increased the crystallization rate of PLA. This increment led to higher crystallinity degree and the formation of different types of crystallites. As a result, the tensile strength and modulus along with the toughness of PLA were improved.[26] The isothermal crystallization of the PLA/BP control sample in the presence of EGs was studied by the isothermal DSC experiment. The obtained thermograms are shown in Fig. 14(a). As can be observed, the crystallization peak of PLA shifts to lower times for PLAEGS3 and PLAEGL3 samples, especially the PLAEGL3 one. For the quantitative analysis of the PLA crystallization rate, the relative degree of crystallization, $X_c(t)$ as a function of time is determined by integrating the area under the crystallization peaks, as follows:

$$X_c(t) = \frac{\int_{t_0}^{t} (dH_c/dt)dt}{\int_{t_0}^{t_\infty} (dH_c/dt)dt} \quad (1)$$

where dH_c is the enthalpy related to the infinitesimal time range of dt. t_0 and t_∞ represent the initial and final crystallization times, respectively. The curves of $X_c(t)$ *versus* time are shown in Fig. 14(b) for different samples. The Avrami theoretical model is applied here to evaluate the EGs effect on the isothermal crystallization kinetics of PLA. According to this model, the equations given below are used to fit the data:

$$X_c(t) = 1 - \exp(-Kt^n) \quad (2)$$

Table 2 Avrami parameters obtained from fitting the model on the experimental data shown in Fig. 14

Sample	n	$K\ (s^{-n})$
PLA/BP	3.46	5.7×10^{-12}
PLAEGL3	2.86	9.3×10^{-10}
PLAEGM3	3.45	4.7×10^{-12}
PLAEGS3	3.14	9.5×10^{-11}

$$\log[-\ln(1 - X_c(t))] = \log K + n \log t \quad (3)$$

where n and K are the Avrami exponent and crystallization constant rate. The Avrami exponent depends on the nucleation mechanism and crystal growth dimensions.[27] The Avrami kinetic parameters, n and K can be calculated from the slope and intercept of $\log[-\ln(1 - X_c(t))]$ *versus* $\log t$ curves. The obtained data are collected in Table 2. The Avrami exponents of samples are around 3, indicating the 2- and 3-dimensional growth of crystals and mixed heterogenous/homogeneous nucleation.[28,29] Just the presence of EGL nanoparticles reduces the Avrami exponent to a value less than 3, demonstrating the assisted nucleation stage of the PLA crystallization by the solid surfaces of EGL nanoparticles. The higher crystallization rate of PLA macromolecules in the presence of EGs can be further clarified by comparing the crystallization rate constant, K. The larger K values are obtained by the addition of EGS and EGL, whereas the rate constant does not show any noticeable changes in the presence of EGM nanofiller. The EGL nanolayers, with larger interfacial area between PLA matrix and filler, accelerate the PLA crystallization by providing heterogeneous nucleation sites. While for the EGS nanofiller with poor delamination state, it seems that the growth stage of the isothermal crystallization is mostly affected. As verified by the rheological test results, the PLA molecular motion is faster in the presence of EGS, hence resulting in higher crystal growth rate. Therefore, both EGL and EGS nanofillers increase the overall crystallization rate of PLA,

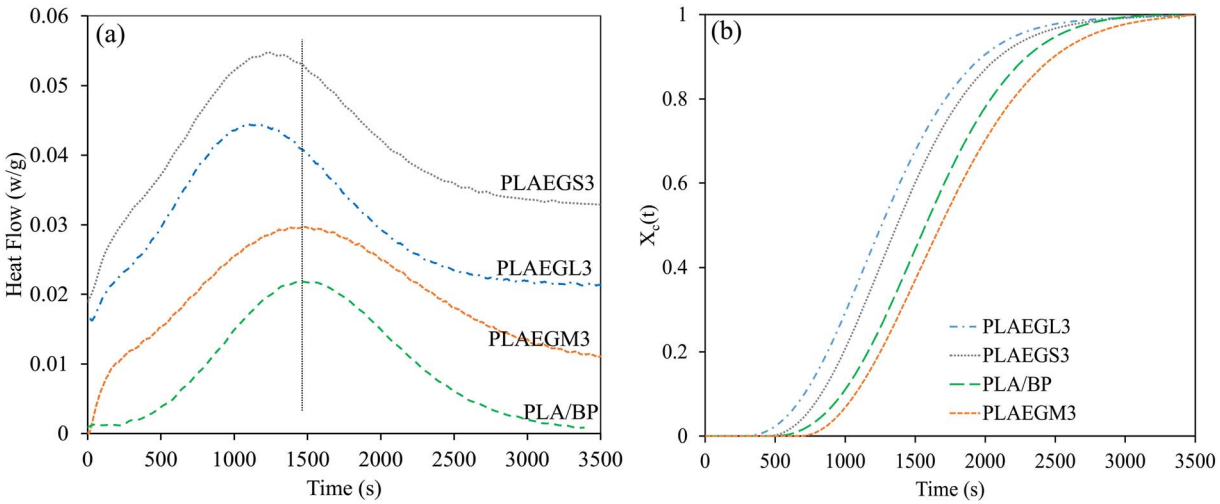

Fig. 14 (a) Heat flow *versus* time for the isothermal crystallization of samples at 118 °C (Exo up), (b) degree of crystallization against time for the thermograms shown in (a).

but through participating in different stages of the PLA crystallization. The higher crystallization rate can result in the formation of PLA crystallites at larger quantities and sizes.[25,26,30] Therefore, the PLA/EGM nanocomposites, especially at lower nanofiller loadings, show higher impact strength owing to larger unaffected tie molecules in the amorphous state. The addition of EGS filler to the PLA/BP sample comparatively causes the lowest Young modulus and tensile strength, though the elongation at break and tensile dissipated energy of PLA/EGS samples are a bit higher than the ones for the PLA/EGM nanocomposites.

The plausible reason of these data is the faster PLA molecular motion in the PLA/EGS nanocomposite comparing with the PLA/EGM systems. However, the incorporation of EGL nanoparticles into PLA/BP brought about the largest dissipated energy and ultimate strain in the tensile tests. On the other hand, the PLAEGL3 nanocomposite show the highest PLA crystallization rate and the slowest PLA relaxation times. These opposing trends are related to the EGL nanoparticle interference on the chemical reactions between benzoyl peroxide and PLA chains. To confirm that, GPC analysis was carried out on the processed virgin PLA sample as well as PLA/BP and PLAEGL3 samples. The molecular weight distribution graphs of these samples are shown in Fig. 15.

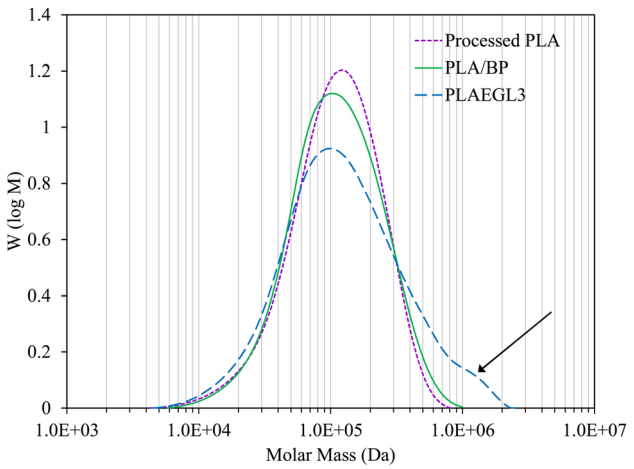

Fig. 15 GPC chromatogram of control samples and PLAEGL3 nanocomposite.

Table 3 Number- and weight-average molecular weight along with polydispersity index (PDI) of samples

Sample	$\bar{M}_n$ (Da)	$\bar{M}_w$ (Da)	PDI
Processed virgin PLA	8.0×10^4	1.4×10^5	1.75
PLA/BP	7.8×10^4	1.5×10^5	1.86
PLAEGL3	7.8×10^4	2.1×10^5	2.67

The measured average molecular weights and polydispersity index (PDI) of samples are gathered in Table 3. Benzoyl peroxide as a common free-radical initiator can begin several chemical reactions, which can result in the formation of the extended PLA macromolecules with higher molecular weights. By the chemical activity of BP initiator, branched and crosslinked PLA macromolecules can be formed. The scheme of the related chemical reactions is shown in Fig. 16. The reason of BP use in the process is the chain scission of PLA chains during the melt processing, which deteriorates the final performance of the PLA-based products. In order to compensate the adverse effects of the inevitable PLA chain scission during the melt-compounding process, BP additive at a low level was used.

As can be found from Fig. 15 and Table 3, the addition of benzoyl peroxide to virgin PLA causes a slight decrease in the number-average molecular weight ($\bar{M}_n$) and a slight increment in the weight-average molecular weight ($\bar{M}_w$) of PLA, demonstrating the chain extension activity of BP. The exothermic nature of the BP-induced reactions results in lower $\bar{M}_n$. However, the free-radical reactions of grafting the PLA chains onto the other chains causes the larger $\bar{M}_w$ and PDI. The most notable point of GPC analysis is that the EGL nanoparticles intensify the chain extension activity of BP. As can be observed, the presence of EGL nanoparticles considerably increases the $\bar{M}_w$ of PLA macromolecules, while it does not reduce the $\bar{M}_n$ of PLA/BP sample. The arrow in Fig. 15 marks the formation of larger PLA macromolecules in the presence of EGL. The formation of PLA molecules with higher molecular weight leads to higher strain at break and tensile dissipated energy than the control sample, PLA/BP. This phenomenon originates from the

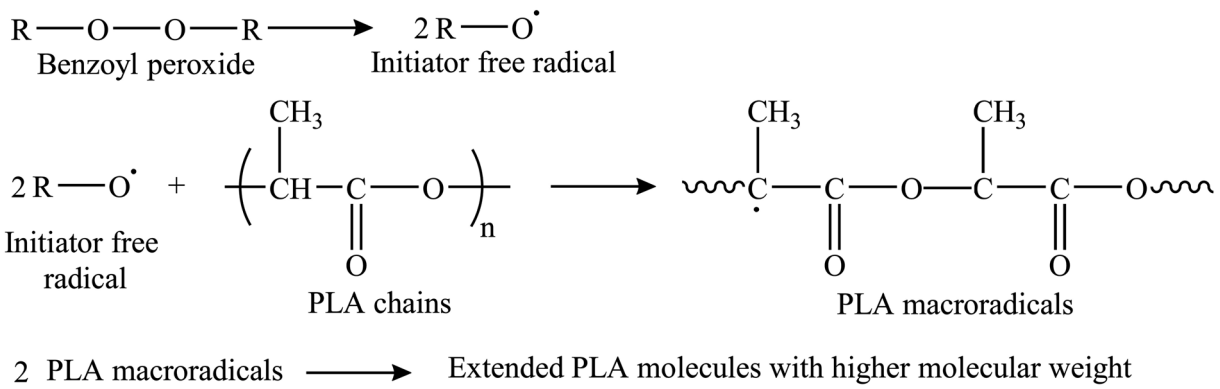

Fig. 16 Probable reaction scheme of benzoyl peroxide and PLA for extending the PLA chains.

effects of EGL nanoplatelets on the rheological properties of PLA during melt-compounding process including higher released shear viscous heat. As a result of that, free-radical grafting reaction is intensified. Different changes in the mechanical and thermo-mechanical properties of extended PLA were observed by adding EGs with different sizes, aspect ratio and dispersion states. Applied EGs impact the PLA crystallization rate and molecular motions as well as PLA molecular weight and structure. Overall, among different used EGs, EGL nanofiller with the highest aspect ratio and filler/matrix interfacial area influences the PLA microstructure, molecular weight and final properties the most.

5. Conclusions

In this research, biodegradable nanocomposites based on poly(lactic acid), benzol peroxide initiator and expanded graphites were prepared using a twin-screw extruder. The effects of EG loading and aspect ratio on the morphology, mechanical and thermo-mechanical properties of extended PLA/EG nanocomposites were investigated. The findings demonstrated that after the graphite pretreatment and thermal shock, EGL expanded the most and the most delamination happened for this type of used graphite. On the other hand, the EGS graphite nanolayers were not well separated from each other and these factors caused the EGL nanocomposites to have a better dispersion and consequently largest interface with the matrix in comparison to the other prepared nanocomposites. Due to the better interactions between EGL and PLA matrix, the best reinforcing effect was observed for the samples containing EGL and the highest modulus and tensile strength were achieved. In these results, it was observed that by adding EGL type graphites, the modulus improved by 44% and the strength enhanced up to 37% compared to the control sample. The highest elongation at break and dissipated energy in tensile test were also determined for PLA/EGL nanocomposites, while the PLA/EGM nanocomposites at lower EG loadings showed larger impact strength than PLA/EGL samples. Among different used EGs, the addition of EGS nanofiller to PLA/BP led to the weakest mechanical and thermos-mechanical performance. The observed changes in the PLA/BP properties by applying EGs originated from the filler/matrix interactions, the PLA crystallization rate affected by the nanofillers, restricted PLA molecular movements and intensified BP initiator activity in extending the PLA chains. EGL, among the other types of EGs, had the strongest impact on the mechanical properties along with the PLA crystallization kinetic, molecular movements and molecular weight.

Conflicts of interest

There are no conflicts to declare.

References

1 J. Julien, J.-C. Quantin, J.-C. Bénézet, A. Bergeret, M. Lacrampe and P. Krawczak, *Eur. Polym. J.*, 2015, **67**, 40–49.
2 M. Nofar and C. B. Park, *Prog. Polym. Sci.*, 2014, **39**, 1721–1741.
3 E. Castro-Aguirre, F. Iniguez-Franco, H. Samsudin, X. Fang and R. Auras, *Adv. Drug Delivery Rev.*, 2016, **107**, 333–366.
4 D. Battegazzore, S. Bocchini and A. Frache, *eXPRESS Polym. Lett.*, 2011, **5**, 849–858.
5 I. H. Kim and Y. G. Jeong, *J. Polym. Sci., Part B: Polym. Phys.*, 2010, **48**, 850–858.
6 X. Zhao, Q. Zhang, D. Chen and P. Lu, *Macromolecules*, 2010, **43**, 2357–2363.
7 B. W. Chieng, N. A. Ibrahim, W. M. Z. W. Yunus, M. Z. Hussein and V. Giita Silverajah, *Int. J. Mol. Sci.*, 2012, **13**, 10920–10934.
8 K. Bocz, T. Tábi, D. Vadas, M. Sauceau, J. Fages and G. Marosi, *eXPRESS Polym. Lett.*, 2016, **10**, 771–779.
9 M. Nofar, *Mater. Des.*, 2016, **101**, 24–34.
10 R. B. Valapa, G. Pugazhenthi and V. Katiyar, *RSC Adv.*, 2015, **5**, 28410–28423.
11 S. Kashi, R. K. Gupta, T. Baum, N. Kao and S. N. Bhattacharya, *Mater. Des.*, 2016, **95**, 119–126.
12 M. E. Mngomezulu, A. S. Luyt and M. J. John, *J. Thermoplast. Compos. Mater.*, 2019, **32**, 89–107.
13 R. Al-Itry, K. Lamnawar and A. Maazouz, *Eur. Polym. J.*, 2014, **58**, 90–102.
14 W. Liu, X. Wang, H. Li, Z. Du and C. Zhang, *J. Cell. Plast.*, 2013, **49**, 535–554.
15 W. Liu, P. Chen, X. Wang, F. Wang and Y. Wu, *Cell. Polym.*, 2017, **36**, 75–96.
16 S. M. H. Khademi, F. Hemmati and M. A. Aroon, *Int. J. Biol. Macromol.*, 2020, **157**, 470–483.
17 S. Alam, M. F. Mina, M. J. Rahman, M. A. Gafur, K. H. Maria, T. Mieno, A. M. Alam and M. D. H. Beg, *Polym. Polym. Compos.*, 2019, **27**, 20–32.
18 D. M. Cecílio, M. L. Cerrada, E. Pérez, A. Fernandes, J. P. Lourenço, T. F. McKenna and M. R. Ribeiro, *Eur. Polym. J.*, 2023, **184**, 111765.
19 J. George and H. Ishida, *Prog. Polym. Sci.*, 2018, **86**, 1–39.
20 E. Ojogbo, C. Tzoganakis and T. H. Mekonnen, *Composites, Part A*, 2021, **149**, 106580.
21 G. P. Baeza, J. Oberdisse, A. Alegria, K. Saalwächter, M. Couty and A.-C. Genix, *Polymer*, 2015, **73**, 131–138.
22 D. Veigel, K. Rishi, U. Okoli, G. Beaucage, J. A. Galloway, H. Campanelli, J. Ilavsky, I. Kuzmenko and M. Fickenscher, *Polymer*, 2023, **269**, 125735.
23 J. Liu and H. Liang, *Polym. Bull.*, 2022, **79**, 7923–7937.
24 T. Nazari and H. Garmabi, *J. Appl. Polym. Sci.*, 2016, **133**(44), 44120.
25 A. K. Pal and V. Katiyar, *Biomacromolecules*, 2016, **17**, 2603–2618.
26 A. A. Seraji, F. Goharpey and J. Khademzadeh Yeganeh, *J. Appl. Polym. Sci.*, 2022, **139**, e52871.
27 Z. Mohtaramzadeh, F. Hemmati, S. F. Kasbi, V. Goodarzi, K. Arnhold and H. A. Khonakdar, *Polym. Test.*, 2020, **89**, 106593.
28 A. Balazs, *Commun. – Sci. Lett.*, 2017, **19**, 15–19.
29 V. Hinrichs, G. Kalinka and G. Hinrichsen, *J. Macromol. Sci., Part B: Phys.*, 1996, **35**, 295–302.
30 J. L. Alves, P. T. V. e Rosa, V. Realinho, M. Antunes, J. I. Velasco and A. R. Morales, *Appl. Clay Sci.*, 2019, **180**, 105186.